J Mater Sci (2008) 43:4742–4748
DOI 10.1007/s10853-007-2357-4

REACTIVITY OF SOLIDS

Synthesis and characterization of layered and scrolled amine-templated vanadium oxides

Megan Roppolo · Christopher B. Jacobs · Shailesh Upreti · Natasha A. Chernova · M. Stanley Whittingham

Received: 14 September 2007 / Accepted: 27 November 2007 / Published online: 30 April 2008

Abstract In order to fully understand the formation mechanism, structure, and role of structural curvature of vanadium oxide nanotubes (VONTs), two isostructural materials (one planar and the other curved)—ethylenediammonium (enH_2) intercalated V_7O_{16} and vanadium oxide nanourchins (VONUs)—were synthesized and characterized via X-ray diffraction (XRD), electron microscopy, thermal gravimetric analysis (TGA), Fourier transform infrared spectroscopy, and magnetic measurements. The synthesis route to $(enH_2)V_7O_{16}$ is developed using vanadium pentoxide as a starting material and employing pH control. VONUs are synthesized using n-dodecylamine as an amine template for the first time. We demonstrate that the structure of the vanadium oxide layer in these compounds is similar to that of VONTs and their magnetic properties all fit to the same model including the temperature-independent, Curie–Weiss, and spin ½ antiferromagnetic dimer contributions. The vanadium oxidation state in tubular structures appears to be higher than in planar compounds such as $(eH_2)V_7O_{16}$ and BaV_7O_{16}. The role of the template and vanadium reduction in the formation of nanotubes is discussed.

Introduction

Vanadium oxides have been studied extensively because their layered structures and redox activity make them candidates for use as cathode materials in lithium batteries, as well as for catalysis and sensor applications [1–3]. A variety of structures are possible, because vanadium has several oxidation states with various oxygen coordination that can coexist in the same crystal [4]. Many of the layered and open-framework structures that are most desirable for the applications mentioned are metastable phases that can be formed through the use of hydrothermal synthesis. This method employs relatively low temperatures (150−200 °C) and allows for the formation of many templated vanadium oxide phases [5].

Vanadium oxide nanotubes (VONTs), first synthesized by Spahr et al. [6] are an interesting example of a phase where a long-chain amine is used as a template. These nanostructured materials are of particular interest because of their high surface area, with reactive sites on the inside and outside of the tube and along the opening, as well as for their ability to perform redox reactions [7–9]. Despite these desirable properties, the exact mechanisms by which VONTs form and grow are not yet understood in full. It is for this reason that we present this study of two VONT-related structures, $(enH_2)V_7O_{16}$ and vanadium oxide nanourchins (VONUs) [10, 11].

The tubular morphology of VONTs does not allow them to fit in a typical unit cell, meaning that the structure of VONT walls cannot be fully characterized by traditional crystallographic techniques [7]. The wall structure of VONTs is believed to be related to the vanadium oxide layer of BaV_7O_{16}, based on the similar tetragonal unit cell with the intralayer cell parameter $a \approx 6.2$ Å [12]. The pair-distribution function analysis confirms the similarity of these two structures [7]. The $(enH_2)V_7O_{16}$ crystallizes in a triclinic structure with close $a = 6.16$ Å and $b = 6.17$ Å cell parameters, and a similar vanadium and oxygen arrangement to BaV_7O_{16} and VONT walls. However, the

M. Roppolo · C. B. Jacobs · S. Upreti · N. A. Chernova (✉) · M. S. Whittingham
Department of Chemistry and Institute for Materials Research, State University of New York at Binghamton, Binghamton, NY 13902-6000, USA
e-mail: nchernova@gmail.com

intercalated short-chain ethylenediammonium does not allow for scrolling or rolling of the layered oxide [10]. Neither the Ba nor the (enH_2) intercalated V_7O_{16} compound has been obtained as a pure phase in an amount significant enough to allow extensive properties studies [10, 12]. The present work was motivated by this fact, as the ability to study this structure could allow us to elucidate the charge distribution and the mechanism of formation of VONTs.

The novel vanadium oxide nanourchin morphology, which consists of a radial array of VONTs, may give us helpful insights on the direction of nanotube growth. O'Dwyer et al. proposed that nanourchin formation begins with a lamellar precursor, which aggregates into a collection of lamellar pieces [11]. Only then do nanotubes form and grow into an urchin of 9–12 μm in diameter, suggesting that the direction of VONT growth is along the length of the tube. So far, only hexadecylamine-templated nanotubes were reported to form the urchin morphology. We have attempted the VONU synthesis using dodecylamine with the aim of determining whether the amine length is critical for the formation of urchins and to facilitate the comparison of properties with VONTs, many of which are dodecylamine-templated.

Experimental details

The synthesis of $(enH_2)V_7O_{16}$ was derived from the procedure outlined by Nesper et al. [10]. In a stoppered flask, a 2:1 molar ratio of V_2O_5 and ethylene diamine was stirred in ethanol. After 1 h, reverse osmosis water was added and the mixture was stirred for 24 h. The solution pH was adjusted with acetic acid before hydrothermal treatment, which was performed in a Teflon™-lined Parr bomb at 180 °C for 7 days. The pH values of 2.4, 3, 4, 5, 7, and 9.6 were tested, with pH 4 syntheses giving $(enH_2)V_7O_{16}$. The resulting black solid was vacuum filtered, rinsed with deionized water and ethanol, and dried in a vacuum oven.

The synthesis of VONUs was carried out according to the procedure described by O'Dwyer et al. replacing hexadecylamine with dodecylamine. Vanadium (V) triisopropoxide (2×10^{-3} mol) was combined with a solution of dodecylamine (10^{-3} mol) in ethanol (10 mL) and stirred vigorously for 1 h under a nitrogen atmosphere [11]. The resulting clear yellow liquid was hydrolyzed with reverse osmosis water (15 mL) in air, precipitating an orange solid. After mixing for 24 h, hydrothermal treatment of the orange suspension was performed in a Teflon™-lined Parr bomb at 180 °C for 7 days. The resulting black solid was vacuum filtered, rinsed with deionized water and ethanol, and dried in a vacuum oven.

Vanadium oxide nanotubes were synthesized for the sake of comparison using Nesper's procedure [13]. A mixture of n-dodecylamine (27.5 mmol) and vanadium pentoxide (27.5 mmol) was dissolved in ethanol (9.1 mL) and stirred for 2 h. Water (26 mL) was added dropwise to the solution while continuously stirring. The mixture was allowed to age for 24 h until a complete color change from mustard to brown-orange was observed. The mixture was transferred into a Teflon-lined stainless steel Parr bomb and was heated at 185 °C for 7 days. After the reaction, the system was slowly cooled to room temperature. A fluffy black solid was observed and was vacuum rinsed with 75 mL each of hexane, acetone, and reverse osmosis water. The solid was then dried overnight under vacuum at 80 °C. The composition of obtained VONTs is $(C_{12}H_{25}NH_3)_{0.3}VO_{2.36}$ as determined by thermal gravimetric analysis (TGA) in oxygen, and carbon, hydrogen, nitrogen (CHN) elemental analysis.

All products were characterized using powder X-ray diffraction (XRD), transmission and scanning electron microscopy (TEM and SEM), and other methods to ensure single-phase products. Room temperature XRD data were collected using a Scintag diffractometer with Ni-filtered Cu K_α radiation. Data were collected in a continuous manner with a speed of 0.75°/min over the range $2° < 2\theta < 90°$. A Hitachi H-7000 transmission electron microscope at an accelerating voltage of 100 kV was used on samples mounted on a carbon-coated 400-mesh copper grid after suspension in anhydrous hexane. For SEM images, a Hitachi 570LB scanning electron microscope was used. TGA was carried out on a Perkin-Elmer model TGA7 in oxygen at a rate of 3 °C/min to determine the water and organic content as well as overall stability. Infrared spectra were obtained with a Perkin-Elmer 1600 series for Fourier Transfer Infrared Spectroscopy (FTIR) using a KBr pellet as background. The temperature dependences of the DC magnetization were measured on Quantum Design MPMS-XL5 cooling the samples from either 400 or 350 to 2 K in a magnetic field of 1 T.

Colorimetric titration of the $(enH_2)V_7O_{16}$ sample with potassium permanganate was performed in order to determine the ratio of vanadium oxidation states in the compound. In 50 mL of sulfuric acid with a concentration of approximately 1 M, 0.105 g of $(enH_2)V_7O_{16}$ was dissolved overnight. A blue solution was observed after this period. A corresponding "blank" solution was also produced using all constituents of the original solution except the $(enH_2)V_7O_{16}$ material. Both solutions were then titrated with a 0.006937 M $KMnO_4$ solution until matching light-pink endpoints were reached. The amount of titrant used to reach a pink color in the blank was subtracted from the amount used in the solution containing the sample. The endpoint was reached after the addition of 23.10 mL of titrant. The calculation of the percentages of vanadium 4+ and 5+ states was based on the following reaction with permanganate $5VO^{2+} + MnO_4^- + 6H_2O \rightarrow 5VO_3^- + Mn^{2+} + 12H^+$ [14]. The amount of V^{4+} was calculated to be 73.3%.

Results and discussion

Effect of pH on ethylene diamine-intercalated vanadium oxides

In the synthesis of $(enH_2)V_7O_{16}$, the standard VONT synthesis procedure was coupled with pH control, which is known to affect the oxidation state and coordination of vanadium in hydrothermal synthesis [15]. To this end, identical syntheses were performed at pH values of 2.4, 3, 4, 5, 7, and 9.6. This resulted in the formation of several different phases, which were subsequently studied by powder XRD. The pH 2.4 product consists of one or several phases so far unidentified. The desired $(enH_2)V_7O_{16}$ phase, which simulates the makeup of VONT walls, was found in the products synthesized at pH values of 3, 4, 5, and 7. The XRD has revealed only the peaks attributed to $(enH_2)V_7O_{16}$ for the pH 4 product. At pH 3, two additional low-angle peaks of low intensity are observed, indicating the presence of minor impurities or the imperfect layered structure of the $(enH_2)V_7O_{16}$ formed. For the pH 5 and 7 compounds, XRD studies show that the $(enH_2)V_7O_{16}$ phase is mixed with another known phase, β-$(enH_2)V_4O_{10}$ [16]. This same phase was present as an impurity in the original report on $(enH_2)V_7O_{16}$ [10]. The β-$(enH_2)V_4O_{10}$ phase is also present in pH 9.6, though $(enH_2)V_7O_{16}$ is not. At the last three pH values (5, 7, 9.6), at least one more phase is present that is yet uncharacterized.

The obtained results further confirm the trends that were first observed in the $NMe_4-V_2O_5$–LiOH system [15]. With decreasing pH, the coordination of vanadium changes from the tetrahedral- and square-pyramidal configuration found in β-$(enH_2)V_4O_{10}$ to the tetrahedrons and distorted octahedrons found in $(enH_2)V_7O_{16}$. The vanadium coordination change reflects the site preference for different vanadium oxidation states: V^{5+} is usually found in tetrahedral sites, V^{4+} coordination is either square-pyramidal or octahedral, V^{3+} adopts octahedral coordination. Indeed, the β-$(enH_2)V_4O_{10}$ contains vanadium ions with the average oxidation state of $V^{4.5+}$, which are less reduced than the lower pH phase $(enH_2)V_7O_{16}$, where the average oxidation state is $V^{4.3+}$. Following this logic, the unidentified phase obtained at pH 2.4 is likely to contain even more reduced vanadium, probably V^{4+}, in octahedral oxygen coordination.

Characterization of $(enH_2)V_7O_{16}$

The powder XRD pattern of the layered compound $(enH_2)V_7O_{16}$ synthesized at pH 4 was compared to single-crystal data obtained by Nesper's group using the Rietveld method (Fig. 1). It was determined that the data conforms to the expected $P\bar{1}$ space group with lattice parameters of $a = 6.167(2)$ Å, $b = 6.170(2)$ Å, $c = 19.107(5)$ Å, and angles $\alpha = 96.062(7)°$, $\beta = 92.66(1)°$, $\gamma = 90.011(6)°$. The low R_p value of 0.077 and the absence of any additional peaks in the experimental pattern suggest that the two patterns are a match and support the claim that $(enH_2)V_7O_{16}$ is the only phase formed. The corresponding SEM image in Fig. 2a shows only crystals of approximately 1–2 μm with the expected plate-like morphology that have grown together to form rosette-like conglomerates.

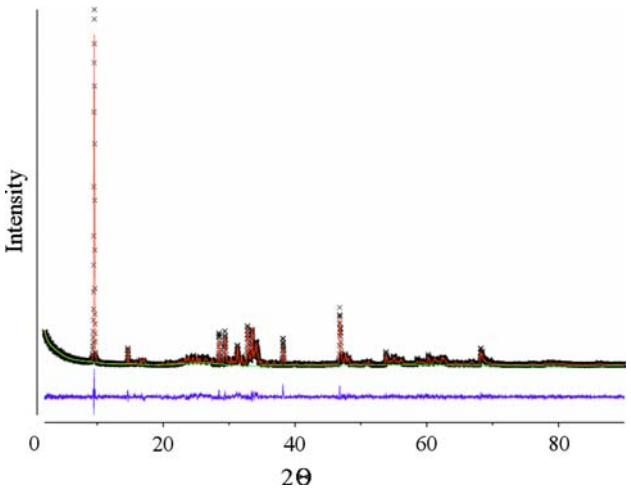

Fig. 1 X-ray diffraction pattern of $(enH_2)V_7O_{16}$ synthesized at pH 4 (black crosses), its Rietveld refinement (red line) and their difference (blue line)

Thermal gravimetric analysis data in Fig. 3 shows a one-step weight loss of 6.9% in oxygen between 200 °C and 350 °C resulting in V_2O_5. The expected weight loss in oxygen is 5.7%, which is consistent with the experimentally observed value. The amine content was further verified by the CHN analysis. This analysis gives enH_2 content of 9.5 wt.%, consistent with 9.2 wt.% expected for $(enH_2)V_7O_{16}$ chemical composition; the experimental (calculated) weight percentages are 3.97 (3.56) for C, 1.54 (1.48) for H, and 3.98 (4.15) for N. The overall chemical composition determined from the CHN analysis and TGA in oxygen is $(enH_2)_{1.0 \pm 0.1}V_7O_{16.0 \pm 0.1}$.

Formation of vanadium oxide nanourchins

Synthesis of VONUs starts with the formation of a layered precursor by the hydrolysis and subsequent aging of a solution of vanadium (V) triisopropoxide and dodecylamine in ethanol. This step is consistent with the original VONT synthesis; however, the amounts of ethanol and water used in urchin synthesis are, respectively, 75 and 15 times as much as in VONT synthesis per equal amount of vanadium. The diluted conditions allow the VONTs to grow in all directions from the urchin nucleation site to reach several microns in length. Sampling of the mixture periodically throughout the aging process allowed us to follow the formation of layered

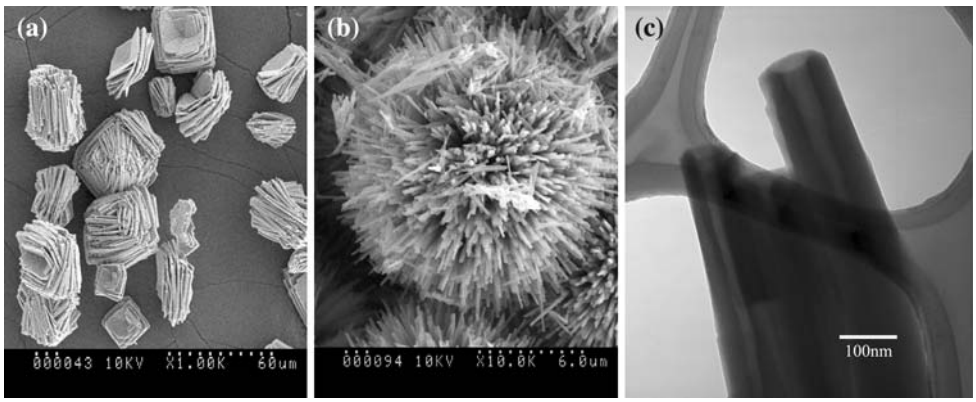

Fig. 2 Electron microscopy images: (**a**) an SEM image of $(enH_2)V_7O_{16}$ synthesized at pH 4, (**b**) an SEM image of a vanadium oxide nanourchin synthesized with dodecylamine, and (**c**) a TEM image of the dodecylamine nanotubes present in a nanourchin

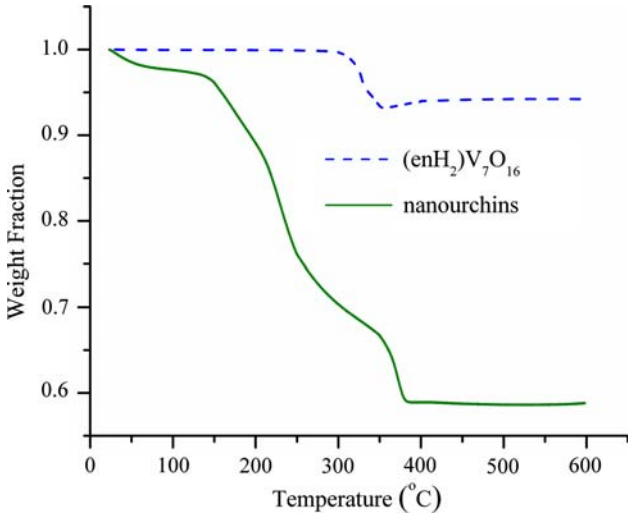

Fig. 3 TGA in O_2 of $(enH_2)V_7O_{16}$ synthesized at pH 4 and vanadium oxide nanourchins synthesized with dodecylamine

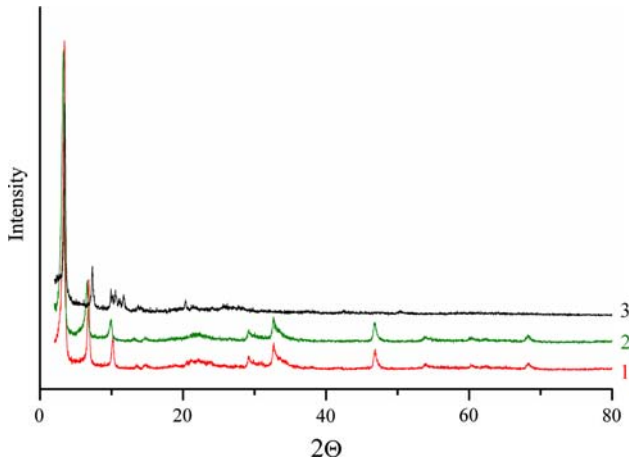

Fig. 4 The X-ray diffraction patterns of (1) the VONTs, (2) the urchins, and (3) the layered structure synthesized using dodecylamine

precursor from vanadium triisopropoxide and dodecylamine. In less than 12 h, sharp peaks are observed at low angles in the XRD spectrum of the mixture; and after 24 h of aging, a layered compound with d-spacing of about 26.2 Å is formed (Fig. 4). During this time, the mixture changes color from bright orange upon the addition of water to a yellow-brown after 24 h. This aged mixture then undergoes hydrothermal treatment, forming the final nanourchin product.

The powder XRD spectrum for nanourchins containing dodecylamine is similar to that of VONTs with the same amine surfactant (Fig. 4). Unit cell parameters were calculated as $a = 6.110(1)$ Å and $c = 26.6(2)$ Å for nanourchins and $a = 6.151(2)$ Å and $c = 27.2(2)$ Å for VONTs. The SEM image (Fig. 2b) shows that urchins of 9–12 μm in diameter are the major synthesis product; however, occasional VONTs are also found. The TEM image in Fig. 2c confirms that nanourchins are made up of high-quality VONTs. The better quality of VONTs assembled in urchin morphology compared to that of regular VONTs was also found by O'Dwyer for the hexadecylamine-templated compounds [11].

The nanourchin TGA results (Fig. 3) show a weight loss of 41.5% between 140 °C and at 300 °C in oxygen. A chemical composition of $(C_{12}H_{25}NH_3)_{0.34}VO_{2.36}{\cdot}0.2H_2O$ or $(C_{12}H_{25}NH_3)_{2.4}V_7O_{16.5}{\cdot}1.4H_2O$ was calculated for the nanourchins and was confirmed by CHN elemental analysis. The observed (calculated) weight percentages are 31.72 (31.45) for C, 6.10 (6.37) for H, and 2.78 (3.06) for N. It should be noted that this chemical composition differs somewhat from the $(C_{16}H_{33}NH_3)_{0.42}VO_{2.5}{\cdot}1.8H_2O$ obtained by O'Dwyer. The principal difference comes from the fact that our analysis accounts for the possible oxygen non-stoichiometry. We find that the oxygen content in the nanourchins as well as the organic template content are close to that reported for dodecylamine-templated VONTs $(C_{12}H_{25}NH_3)_{0.28}VO_{2.4}$ [13]. This aspect will be further discussed in the magnetic properties section.

FTIR studies

The FTIR spectra of $(enH_2)V_7O_{16}$, urchins and VONTs presented in Fig. 5 confirm the structural similarity of these compounds. The strong absorption at 2,850 and 2,920 cm^{-1}

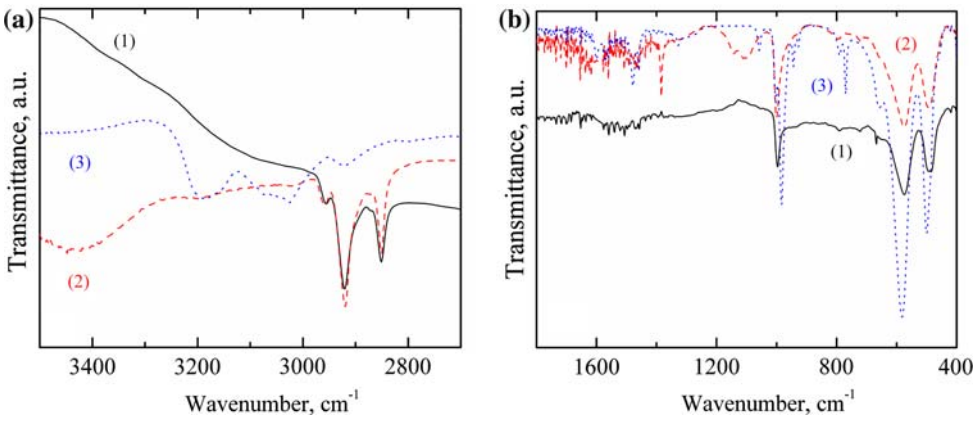

Fig. 5 FTIR spectra of (**a**) C–H and N–H regions and (**b**) V–O region for (1) VONTs (2) nanourchins, and (3) $(enH_2)V_7O_{16}$

can be attributed to stretching modes of C–H vibrations in $C_{12}H_{25}NH_3^+$ and enH_2^{2+}. The absorption near 3,400 cm^{-1}, typical of $–NH_2$ groups, is absent in all compounds except urchins, while absorption near 3,000 cm^{-1}, observed for $(enH_2)V_7O_{16}$, and near 1,600 cm^{-1}, present in all spectra, indicates that the amines are protonated in all cases. The absorption at 3,400 cm^{-1} in the nanourchin spectrum may be attributed to O–H stretching vibrations due to the presence of water [17]. The FTIR spectra in the 500–1,000 cm^{-1} region, where V–O lattice vibrations signatures are found, are very similar for VONTs and urchins. The strong bands are observed at 484, 579, and 998 cm^{-1}, which is consistent with previous reports [8, 10, 18, 19]. The $(enH_2)V_7O_{16}$ also contains the first two of the above-mentioned three bands, but they are slightly shifted toward higher wavenumbers, appearing at 499 and 584 cm^{-1}. These bands are related to V–O–V bonding, which appears to be stronger in $(enH_2)V_7O_{16}$. The third band, attributed to the V = O stretching vibrations of the vanadyl groups, splits into four bands in $(enH_2)V_7O_{16}$ at 1,003, 982, 943, and 926 cm^{-1}, which reflects the presence of four non-equivalent V = O groups with bond lengths of 1.584, 1.598, 1.627 and 1.656 Å. The BaV_7O_{16} structure has only one type of V = O group with a bond length of 1.600 Å. In the VONTs, the vanadyl groups are likely to become nonequivalent due to curvature, but according to Nesper's data, the difference in bond length is not as dramatic as in $(enH_2)V_7O_{16}$: 1.600 and 1.610 Å [10]. Generally, the larger number of absorption bands observed in $(enH_2)V_7O_{16}$ reflects the lower crystallographic symmetry of this compound and higher number of different V–O bonds.

Magnetic properties

Vanadium oxide nanotubes exhibit very interesting magnetic properties which are currently not quite understood [20]. At low temperatures, a Curie–Weiss paramagnetism is observed, while above 100 K, there is a susceptibility maximum, typical of low-dimensional magnetic behavior. The high temperature of this maximum indicates strong antiferromagnetic exchange between vanadium ions. This maximum can be described by a model of antiferromagnetic S = 1/2 dimers, i.e., two V^{4+} ions located structurally close to each other, either sharing corners or edges, but not interacting magnetically with other V^{4+} ions [20, 21]. The existence of such dimers is not evident from a structural point of view. The other challenge the V_7O_{16} vanadium layer poses is the location of paramagnetic V^{4+} ions, i.e., those that are not magnetically ordered and not strongly interacting. The original work on BaV_7O_{16} suggests, on the basis of a bond valence sum calculation, that V^{4+} ions occupy tetrahedral sites; the details and the structure figure may be found in Ref. [12]. However, the tetrahedral site is unusual for V^{4+} ion, preferring larger square-pyramidal or octahedral coordination. Magnetic properties of BaV_7O_{16} have never been reported, therefore magnetism of related $(enH_2)V_7O_{16}$ as well as VONTs and urchins is of interest.

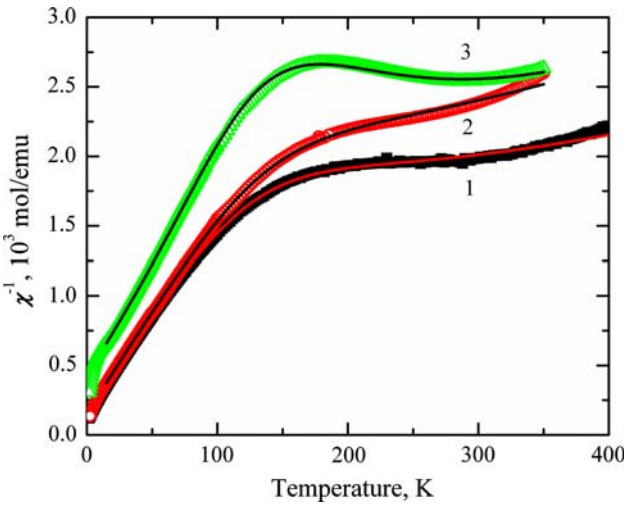

Fig. 6 Reciprocal magnetic susceptibilities of (1) VONTs, (2) vanadium oxide nanourchins, and (3) $(enH_2)V_7O_{16}$. Solid lines represent the best fit to the sum of temperature-independent susceptibility, paramagnetic Curie–Weiss susceptibility and the susceptibility of antiferromagnetic dimers

Table 1 Magnetic properties of vanadium oxide nanotubes (VONTs), nanourchins (VONUs), and $(enH_2)V_7O_{16}$

	Composition	V oxidation state from composition	χ_0,10^{-4} emu/mol	N_{V4+}/N_{Vtotal}	N_{V4+PM}/N_{Vtotal}	Θ, K	J/k, K
VONTs	$(C_{12}H_{28}N)_{0.30}VO_{2.36}$	+4.42	1.20(1)	0.58(5)	0.16(1)	−7.0(1)	645(3)
VONUs	$(C_{12}H_{28}N)_{0.34}VO_{2.36}{\cdot}0.2H_2O$	+4.38	0.60(2)	0.52(7)	0.17(1)	−9.7(1)	643(4)
$(enH_2)V_7O_{16}$	$(C_2N_2H_{10})_{0.14}VO_{2.29}$	+4.29	−0.90(3)	0.84(3)	0.19(1)	−30.4(2)	674(3)

Temperature dependences of the reciprocal magnetic susceptibility for these compounds are presented in Fig. 6. The experimental curves were fitted to the sum of the temperature-independent susceptibility χ_0, the paramagnetic Curie–Weiss susceptibility and the susceptibility of non-interacting, spin S = 1/2 dimers [22]:

$$\chi = \chi_0 + \frac{N_{V^{4+}}g^2\mu_B^2}{k}\left[\frac{N_{V^{4+}PM}S(S+1)}{3(T-\Theta)} + \frac{1-N_{V^{4+}PM}}{T(3+\exp(-2J/kT))}\right] \quad (1)$$

Here N_{V4+} is the total number of V^{4+} ions, g is g-factor, which was fixed at $g = 2$, μ_B is the Bohr magneton, k is the Boltzmann constant, N_{V4+PM} is the fraction of paramagnetic V^{4+} ions, Θ is the Curie–Weiss temperature, and J is the intradimer exchange coupling constant. The resulting parameters are summarized in Table 1. Magnetic properties of VONTs and urchins closely resemble each other. Both show a bit more than half of vanadium ions being in 4+ oxidation state, which is consistent with $V^{4.4+}$ oxidation state following from the sample composition. About 16–17% of total vanadium content is represented by paramagnetic V^{4+} ions. This number is strikingly close to the content of tetrahedral sites in the structure, which is 1/7 or about 14%. Considering that hydrothermally synthesized, organic-templated vanadium oxides usually contain from 1 to 2% of paramagnetic impurities the correspondence is ideal [23]. This supports the suggestion that tetrahedral sites may be occupied by V^{4+} ions. The Curie–Weiss temperature in both cases is small and negative, indicating weak antiferromagnetic exchange between the paramagnetic V^{4+} ions. The exchange parameters for the magnetic dimers are close for VONTs and urchins, and agree with earlier reports [20, 21].

Magnetic properties of $(enH_2)V_7O_{16}$ show the same features as those of VONTs and urchins, and can be described by the same model. The magnetic properties suggest that the V^{4+} ions constitute over 80% of total vanadium content in this compound, which is higher than the chemical composition suggests. We have checked the oxidation state of vanadium using titration, and found 73.3% of V^{4+} quite consistent with 70% suggested by chemical composition. This discrepancy as well as the loose fit of the data in the high-temperature region dominated by the magnetic dimer contribution raises the question of applicability of this simple model. Local tests of magnetic excitations are required to achieve understanding of structure-magnetic properties relations in these complex systems. The magnetic data analysis also reveals a stronger exchange between paramagnetic species and between V^{4+} ions in the dimers for $(enH_2)V_7O_{16}$. This is consistent with increased strength of V–O bonding found from FTIR data analysis.

Conclusion

We have developed a synthesis method for $(enH_2)V_7O_{16}$ using pH control for the hydrothermal reaction. VONUs were synthesized for the first time using dodecylamine as a templating agent. This material shows identical XRD pattern, composition, FTIR spectrum, and magnetic properties to VONTs containing dodecylamine. The structural quality of the nanotubes in the urchin structure is much better compared to regular VONTs. Structural similarity of $(enH_2)V_7O_{16}$, VONTs and nanourchins was demonstrated by XRD and FTIR, which confirmed lower symmetry and more irregular oxygen coordination in triclinic $(enH_2)V_7O_{16}$ than in BaV_7O_{16} and VONTs. Chemical analysis and magnetic properties have revealed that vanadium is less reduced in tubular structures than in $(enH_2)V_7O_{16}$. It may indicate that both V^{4+} and V^{5+} in about equal amounts are required for the layer scrolling, while more reduced compounds, with vanadium oxidation state close to 4+, tend to remain flat. This point requires further investigation and elimination of the amine length effect on the scrolling process.

Acknowledgement The financial support from the National Science Foundation through grant DMR-0705657 is greatly appreciated.

References

1. Chirayil TA, Zavalij PY, Whittingham MS (1996) J Electrochem Soc 143:L193
2. Whittingham MS, Song Y, Lutta S, Zavalij PY, Chernova NA (2005) J Mater Chem 15:3362
3. Nordlinder S, Nyholm L, Gustafsson T, Edstrom K (2006) Chem Mater 18:495

4. Zavalij PY, Whittingham MS (1999) Acta Cryst B 55:627
5. Chirayil T, Zavalij PY, Whittingham MS (1998) Chem Mater 10:2629
6. Spahr ME, Bitterli P, Nesper R, Müller M, Krumeich F, Nissen HU (1998) Angew Chem Int Ed 37:1263
7. Petkov V, Zavalij PY, Lutta S, Whittingham MS, Parvanov V, Shastri S (2004) Phys Rev B 69:085410
8. Dobley A, Ngala K, Yang S, Zavalij PY, Whittingham MS (2001) Chem Mater 13:4382
9. Spahr ME, Stoschitzki-Bitterli P, Nesper R, Haas O, Novak P (1999) J Electrochem Soc 146:2780
10. Wörle M, Krumeich F, Bieri F, Muhr H, Nesper R (2002) Z Anorg Allg Chem 628:2778
11. O'Dwyer C, Navas D, Lavayen V, Benavente E, Santa Ana MA, Gonzalez G, Newcomb SB, Sotomayor Torres CM (2006) Chem Mater 18:3016
12. Wang X, Liu L, Bontchev R, Jacobson AJ (1998) Chem Comm 1009
13. Niederberger M, Muhr H-J, Krumeich F, Bieri F, Gunther D, Nesper R (2000) Chem Mater 12:1995
14. Furman NH (1962) Standard methods of chemical analysis. D. Van Nostrand Company Inc., New York
15. Chirayil TG, Boylan EA, Mamak M, Zavalij PY, Whittingham MS (1997) Chem Comm 33
16. Zhang Y, Haushalter RC, Clearfield A (1996) Inorg Chem 35:4950
17. Conley RT (1966) Infrared spectroscopy. Allyn and Bacon Inc., Boston
18. Azambre B, Hudson MJ, Heintz O (2003) J Mater Chem 13:385
19. Chen W, Mai LQ, Peng JF, Xu Q, Zhu QY (2004) J Mater Sci 39:2625. doi:10.1023/B:JMSC.0000020044.67931.ad
20. Krusin-Elbaum L, Newns DM, Zeng H, Derycke V, Sun JZ, Sandstrom R (2004) Nature 431:627
21. Jacobs C, Roppolo M, Butterworth K, Ban C, Chernova NA, Whittingham MS (2007) Mater Res Soc Proc 988E:QQ03
22. Carlin RL (1986) Magnetochemistry. Springer-Verlag, Berlin, p 75
23. Lutta ST, Chernova NA, Zavalij PY, Whittingham MS (2004) J Mater Chem 14:2922